Elastic and inelastic processes in $H^+ + C_2H_2$ collisions below the 1.5-keV regime

M. Kimura
School of Allied Health Sciences, Yamaguchi University, Ube 755, Yamaguchi, Japan
and Institute of Physical and Chemical Research (RIKEN), Wako, Saitama 351-01, Japan

Y. Li, G. Hirsch, and R. J. Buenker
Theoretische Chemie, Bergische Universität-Gesamthochschule Wuppertal, D-42097 Wuppertal, Germany
(Received 8 July 1996)

Electron capture and direct elastic scattering in collisions of H^+ ions with C_2H_2 molecules are studied by using a molecular representation within a fully quantum-mechanical approach below 1.5 keV. Calculations are carried out at two different molecular configurations: (i) C_{00v} symmetry, in which H^+ approaches the H atom along a C—H bond in the acetylene (C_2H_2), and (ii) C_{2v} symmetry, in which H^+ approaches perpendicularly toward the midpoint between two carbon atoms. We find that electron capture in the C_{00v} symmetry configuration takes place preferentially over that in the C_{2v} symmetry configuration at scattering angles above 15°. The results for the C_{2v} and C_{00v} symmetries are comparable in magnitude below 10°, although the C_{2v} symmetry dominates slightly at still smaller angles. Hence, interferences arising from these molecular configurations in differential cross sections for electron capture and elastic scattering processes are strongly present at angles smaller than a few degrees. Accordingly, the total cross section for the C_{2v} symmetry is larger by a factor of 3 at 1 keV, and the difference widens as the energy decreases to the eV regime. This is because in C_{2v} symmetry, H^+ can have a larger overlap with the charge distribution of the C_2H_2 molecule, thus causing a stronger interaction. [S1050-2947(96)07912-7]

PACS number(s): 34.10.+x, 34.70.+e, 34.20.−b

I. INTRODUCTION

Electron capture in collisions of ions with atoms in the low-keV-energy regions has been one of the most active research areas, experimentally and theoretically, in atomic physics in the last two decades, because it provides information fundamental for atomic and molecular spectroscopy and many-body collision dynamics. The study of electron capture is also important for applications such as astrophysics and fusion research. Relatively comprehensive studies involving a variety of atomic targets, a wide range of collision energies (meV to keV), and various charged projectiles have greatly improved our understanding of electron capture in ion-atom collisions [1,2]. An increasing volume of cross-section data for electron capture is now available for application.

Unlike the situation for atomic targets, both experimental and theoretical studies of molecular targets are scarce. From the theoretical side, the difficulties arising from the complexity of the nonspherical field of a molecule are responsible for this slow development, although some limited but vigorous activity in the chemical-reaction research community has been known for some time. Particularly, recent rapid developments in high-tech research areas such as plasma chemistry and ion implantation urgently require proper theoretical understanding of dynamical aspects as well as the determination of accurate cross-section data, and also the development of optimal experimental conditions in these technological areas.

Only for the H_2 target have limited but relatively extensive studies of the molecular effects on electron capture been reported to date [3–8], but no similar level of theoretical study has been reported for other molecular targets. We have carried out a rigorous theoretical investigation of elastic and electron capture processes in collision of H^+ ions with CH_4 (methane) in the region below a few keV, since this hydrocarbon molecule is abundant in various astrophysical environments, fusion reactors, and plasma-chemistry atmospheres, and is known to play a crucial role in determining various physical effects [9]. Our major findings in this study were: (i) electron capture in the C_{2v} symmetry takes place preferentially over that in the C_{3v} symmetry configuration at scattering angles below 15° at 1.5 keV, (ii) but the situation reverses at larger angles. These findings are important for a further deepening of our level of understanding of electron capture from a molecular target and hence, in related applications.

In this second paper of the series for molecular targets, we report the results for electron capture and direct elastic scattering in collisions of H^+ ions with C_2H_2 molecules for energies below 1.5 keV. Contribution from electron capture with simultaneous target excitation is also examined. Hence, the processes studied are

$$H^+ + C_2H_2 \rightarrow H + C_2H_2^+ \quad \text{(electron capture)} \tag{1a}$$

$$\rightarrow H + C_2H_2^{+*}$$

(electron-capture with simultaneous target excitation) (1b)

$$\rightarrow H^+ + C_2H_2^* \quad \text{(target excitation)}. \tag{1c}$$

We obtain our results by using a molecular orbital expansion method within a fully quantum-mechanical and also a semiclassical formalism. Two molecular configurations are specifically considered to study the effects of molecular ori-

entations on collision dynamics: (i) a proton approaches a H atom along the molecular axis of the C—C bond and (ii) it approaches perpendicularly toward the midpoint of the C—C bond in C_2H_2. The interference arising from different molecular orientations is investigated. We hope that this type of study can shed more light on the dynamics of the molecular orientation effect and also provide guidelines for developing a simple model to describe more complex polyatomic molecular targets. Furthermore, the interferences of various origins are an interesting subject of basic physics, and they form an essential basis for possible use of this technique for material and surface analysis. Schneider *et al.* [10] have studied electronic states of the $[H+C_2H_2]^+$ system by using the similar *ab initio* method we have employed, but they have not reported any dynamical aspect of the collision.

II. THEORETICAL MODEL

Theoretical methods used are standard and have been described in detail elsewhere [1]. Hence, only a brief summary is provided here.

A. Molecular states

The adiabatic potential-energy curves are calculated by means of the multireference single- and double-excitation configuration-interaction (MRD-CI) method [11], with configuration selection and energy extrapolation employing the Table-CI algorithm [12] for efficient handling of Hamiltonian matrix elements for many-electron basis functions (symmetrized linear combinations of Slater determinants). The atomic orbital (AO) basis used for carbon consists of the $(9s5p1d)$ primitive set of Huzinaga [13], contracted to $[5s3p1d]$ by Dunning [14], with additional Rydberg functions of s and p type ($\alpha_s=0.023$, $\alpha_s=0.0055$, $\alpha_p=0.021$, $\alpha_p=0.0049$, and $\alpha_d=0.015$). The hydrogen basis (from the same authors) is $(5s1p)$ contracted to $[3s1p]$.

The calculations are carried out in two different point groups, depending on the approach of the proton toward the acetylene molecule. In the approach along the direction of a C—C bond, the systems have an overall symmetry of C_{00v}. The calculations are done in C_{2v}, an Abelian subgroup of C_{00v}. If H^+ approaches the midpoint of C_2H_2 in a direction perpendicular to the C—C bond, the overall symmetry is C_{2v}, and the calculations are performed directly in this point group.

The CI treatment is based on all configurations that are generated by making either single or double orbital substitutions with respect to a number of key or reference configurations. For the $^1\Sigma^+$ states in the C_{00v} arrangement, the most important reference configurations are listed in Table I together with the respective compositions of the molecular orbitals. Configuration A describes the ground state of the closed-shell C_2H_2 molecule, B–H the electron-capture states with one electron (B–D) or two electrons (E–H) transferred from various C_2H_2 molecular orbitals (MO's) to the approaching H^+, and I–K for C_2H_2 internal excitations to $3s$, $3p$, and $3d$ Rydberg orbitals. The resulting generated set is divided into groups of strongly and weakly interacting configurations, respectively, on the basis of the value of the second-order perturbative energy lowering (ΔE_j) in each case. A selection threshold T is employed to carry out the above separation of configurations into these two categories, which in the present case has an energy value of $T=5.0$ μhartree. The multireference analogue of the Davidson correction [15–17], namely, $[1-\Sigma c_p^2]$ $(E_{\rm Cl}-E_{\rm ref})$, where Σc_p^2 is the sum of the squares of all coefficients of reference configurations in the final CI wave function, $E_{\rm CI}$ is the corresponding total energy, and $E_{\rm ref}$ is the corresponding energy obtained from the small secular equation involving only the reference configurations, is applied to estimate the full CI energy for each state in the AO basis employed.

TABLE I. Most important reference configurations employed in the MRD-CI determination of the $^1\Sigma^+$ potential curves for the collinear HCCH$\cdots$H case. The MO's can be characterized by their leading AO components as $\sigma_{2s}=2s_1+2s_2$, $\sigma_{2s}^*=2s_1-2s_2$, $\sigma_{2p}=2p_{z1}+2p_{z2}$, $\pi_{2p}=2p_{x,y1}+2p_{x,y2}$ with $HC_1C_2H\ldots H$ located on the z axis and the indices referring to the two carbon atoms C_1 and C_2, respectively, as well as $H_{1s}\ldots 1s$ of the approaching H and $C_{3n}=3s$, $3p_\pi$, and $3d_\sigma$ at carbon, respectively.

A	$\sigma_{2s}^2\sigma_{2s}^{*2}\sigma_{2p}^2\pi_{2p}^4$
B	$\sigma_{2s}^2\sigma_{2s}^{*2}\sigma_{2p}^1\pi_{2p}^4H_{1s}^1$
C	$\sigma_{2s}^2\sigma_{2s}^{*1}\sigma_{2p}^2\pi_{2p}^4H_{1s}^1$
D	$\sigma_{2s}^1\sigma_{2s}^{*2}\sigma_{2p}^2\pi_{2p}^4H_{1s}^1$
E	$\sigma_{2s}^2\sigma_{2s}^{*2}\sigma_{2p}^0\pi_{2p}^4H_{1s}^2$
F	$\sigma_{2s}^2\sigma_{2s}^{*0}\sigma_{2p}^2\pi_{2p}^4H_{1s}^2$
G	$\sigma_{2s}^0\sigma_{2s}^{*2}\sigma_{2p}^2\pi_{2p}^4H_{1s}^2$
H	$\sigma_{2s}^2\sigma_{2s}^{*2}\sigma_{2p}^2\pi_{2p}^2H_{1s}^2$
I	$\sigma_{2s}^2\sigma_{2s}^{*2}\sigma_{2p}^1\pi_{2p}^4C_{3s}^1$
J	$\sigma_{2s}^2\sigma_{2s}^{*2}\sigma_{2p}^2\pi_{2p}^3C_{3p}^1$
K	$\sigma_{2s}^2\sigma_{2s}^{*2}\sigma_{2p}^1\pi_{2p}^4C_{3d}^1$

In the practical calculations of eigenvalues and eigenfunctions, all coordinates within the C_2H_2 molecule were frozen at the equilibrium intramolecular distances of the linear geometry: $r_{C\text{-}C}=1.208$ Å and $r_{C\text{-}H}=1.058$ Å [18]. Hence, only the internuclear distance (R) between the H^+ projective and the midpoint of the C-C bond was varied. This approximation should be valid when the collision time is shorter than the vibrational period of the target molecule, as discussed in a previous study of $(H+CH_4)^+$ [9]. In the present case, the approximation is reasonable down to a few tens of eV of collision energy. Furthermore, the geometry of the $C_2H_2^+$ molecular ions formed after electron capture is also frozen at the initial configuration, since including a relaxation of this approximation has little effect on electron capture dynamics.

B. Collision dynamics

Semiclassical approach. A semiclassical MO expansion method with a straight-line trajectory of the incident ion was employed to study the collision dynamics above 50 eV [1]. In this approach, the relative motion of heavy particles is treated classically, while electronic motions are treated quantum mechanically. The total scattering wave function was expanded in terms of products of a molecular electronic state and atomic-type electron translation factors (ETF's), in which the inclusion of the ETF satisfies the correct scattering boundary condition. Substituting the total wave function into the time-dependent Schrödinger equation and retaining the ETF correction up to first order in the relative velocity be-

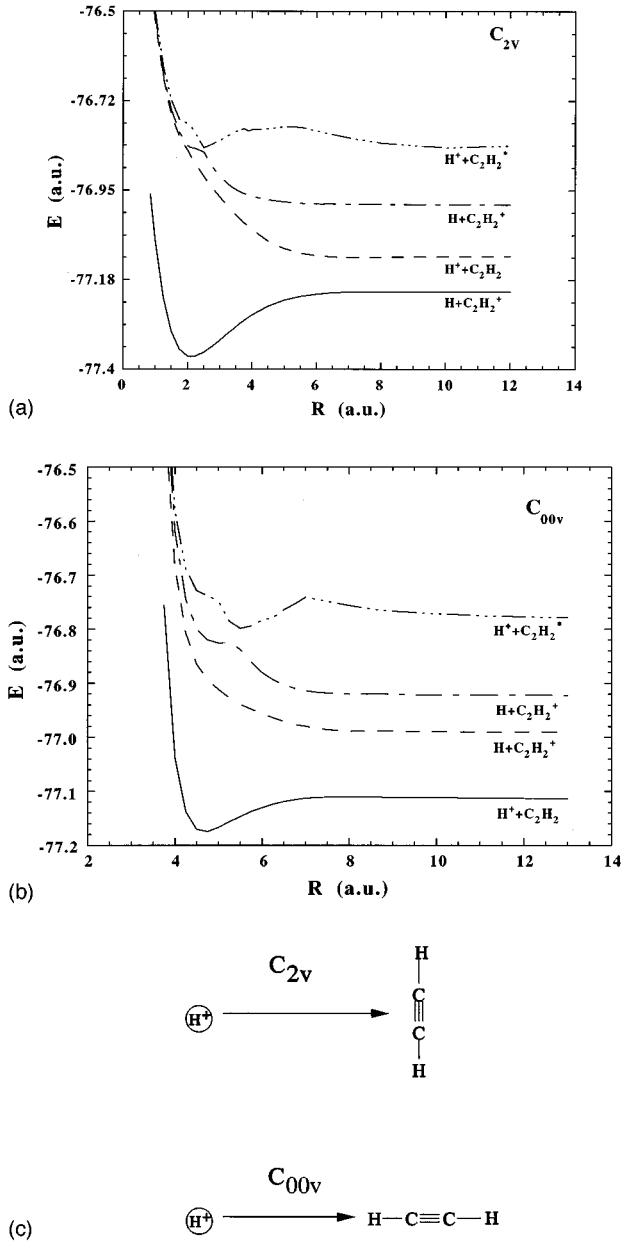

FIG. 1. (a) Adiabatic potential curves for C_{2v} symmetry. (b) Adiabatic potential curves for C_{00v} symmetry. (c) Schematic diagram indicating the molecular configurations for collisions.

tween the collision partners, we obtain a set of first-order coupled equations in time t. Transitions between the molecular states are driven by nonadiabatic couplings. By solving the coupled equations numerically, we obtain the scattering amplitudes for transitions: the square of the amplitude gives the transition probability, and integration of the probability over the impact parameter gives the cross section. The molecular states included in the dynamical calculations are the two sets of states, shown in Figs. 1(a) and 1(b), separating to the initial $[H^+ + C_2H_2]$ channel, various electron capture $[H + C_2H_2{}^+]$, and target-excitation $[H^+ + C_2H_2{}^*]$ channels.

Quantum approach. A fully quantum-mechanical representation of the MO expansion method was employed; that is, dynamical transitions are driven by nonadiabatic couplings [1]. The total wave function for scattering is described as a product of the electronic and nuclear wave functions. Substitution of the total scattering wave function into the stationary Schrödinger equation yields coupled, second-order differential equations for nuclear wave function $X^a(R)$. It is computationally convenient to solve the coupled equations in a diabatic representation [1]. The transformation from the adiabatic to the diabatic representation can be readily achieved through a unitary transformation matrix $C(R)$. In this representation the nuclear wave function for the heavy particles is related to $X^d(R) = C^{-1}X^a(R)$, and the diabatic potential matrix is $V^d = C^{-1}V^aC$, where V^a is the adiabatic potential matrix. The resulting coupled equations for $X^d(R)$ are given in matrix form as

$$[\tfrac{1}{2}\Delta_R I - V^d(R) + EI]X^d(R) = 0, \tag{2}$$

where μ is the reduced mass of the system, I is the identity matrix, and V^d is the diabatic potential matrix. The coupled equations (2) are solved numerically to obtain the scattering S^l matrix for each partial wave l [19]. The differential cross section is then obtained from the standard formula

$$d\sigma/d\Omega = \frac{1}{4k^2}\left|\sum (2l+1)\{\delta_{if} - S^l_{if}\}P_l(\cos\theta)\right|, \tag{3}$$

where S^l_{if} is the scattering S-matrix element for partial wave l, θ is the scattering angle in center-of-mass coordinates, and k is the momentum of the projectile with collision energy $E = k^2/2$. Integration over all angles gives the total cross section. In the present calculation, we employed two- and three-state close-coupling treatments with molecular orbitals corresponding to the initial $[H^+ + C_2H_2]$ and electron capture $[H + C_2H_2{}^+]$ channels.

C. Analysis of oscillatory structures in the cross sections

For some systems, differential cross sections and, sometimes, total cross sections display oscillatory structures as functions of collision energy or scattering angle. A semiclassical analysis for these structures would be sound and would improve our understanding of the underlying physics [20]. To discuss the scattering pattern, the deflection function $\Theta_J(L,E)$ must be determined for each trajectory and potential region J. This function is expressed as

$$\Theta_J(L,E) = \pi - 2b\int_{R_t}[1 - V(R)/E - b^2/R^2]^{-1/2}dR/R^2, \tag{4}$$

where b is the impact parameter and R_t is the inner zero (turning point) of the integrand. The parameter b relates to the orbital angular momentum L by

$$L^2 = 2\mu[E - V(\infty)]b^2, \tag{5}$$

where the classical mechanical quantity is connected to that of quantum mechanics.

III. RESULTS

A. Adiabatic potentials and couplings

Adiabatic potential curves obtained by the procedure outlined in Sec. II A for C_{2v} and C_{00v} symmetries are displayed

in Figs. 1(a) and 1(b), respectively. For C_{2v} symmetry, the lowest level in the figures is an electron-capture state dissociating to the electronic configuration $[H(1s)+C_2H_2^+(^1\Pi_g:1\sigma_1^2 2\sigma_1^2 3\sigma_2^2 1\pi_3^2)]$. The next state corresponds to the initial ground state with the electronic configuration $[H^+ + C_2H_2]$. Then, the electron capture state $[H(1s)+C_2H_2^+]$ and electronically excited $[H^+ + C_2H_2{}^*]$ states follow. For C_{00v} symmetry, the lowest state corresponds to the initial ground $[H^+ + C_2H_2]$ state, and two electron-capture states follow. A target-excitation $[H^+ + C_2H_2{}^*]$ channel lies above these. In both configurations, the first three states from the bottom show typical features in their potential curves, that is, a weakly ionized colliding system in which there is no sharply avoided crossing among these states. As one proceeds to higher levels, the energy defect becomes smaller and, therefore, states begin mixing strongly, resulting in a sharply avoided crossing, as we can see for states above the first four or five levels from the ground state.

For infinite internuclear distance between the projectile and the C_2H_2 molecule, the energy defects between the initial and electron-capture channels for the two symmetries should be equal. However, at finite separations, these values are different. That for the linear symmetry is somewhat smaller, with a value of 0.2127 a.u. at $R=10a_0$, compared to 0.2227 a.u. for C_{2v} symmetry at the same distance. The initial channel has a sharply avoided crossing with the electron-capture channel in the small-R region around $1.0a_0$ and $2.0a_0$ in C_{2v} symmetry, but no obvious avoided crossing is found for C_{00v} symmetry. Consideration of the molecular configuration [Fig. 1(c)] indicates that the H^+ ion can penetrate deep inside the C—C bond in the C_2H_2 molecule, causing strong mixing of electronic states. Hence, the reason for this avoided crossing in C_{2v} symmetry is apparent. Except for this avoided crossing at small R for C_{2v} symmetry, however, the general shapes of the potential curves for the perpendicular and linear approaches are similar, and the constant energy separation at finite R between the initial and electron-capture channels indicates that the collision dynamics are governed mainly by the Demkov-type coupling scheme in this range [1].

The dominant radial couplings are illustrated in Figs. 2(a) and 2(b) for the C_{2v} and C_{00v} symmetries, respectively. As we speculated above, the coupling between 1Σ and 2Σ has a sharp peak at $R=1.0a_0$, reflecting the avoided crossing in C_{2v} symmetry, and this is followed by a second peak near $R=2.0a_0$. This is a typical Landau-Zener-type coupling, and except for these two sharp peaks at small R, the 1Σ-2Σ coupling drops off rapidly at larger R and becomes zero beyond $3a_0$. The 2Σ-3Σ coupling has a weak but broad hump from $2.5a_0$ to $7a_0$, a typical Demkov-type coupling scheme, and it is expected to play a crucial role for electron capture at high energies where the 1Σ-2Σ coupling becomes less effective. Unlike the case for C_{2v} symmetry, the coupling for the linear approach is a single broad peak at $R>5a_0$, again as a consequence of the Demkov-type coupling scheme. This is because the incoming H^+ ions feel little electronic field except that of the H atom, which is directly approached. As one goes to higher levels, the states typically mix strongly with each other, showing a complex

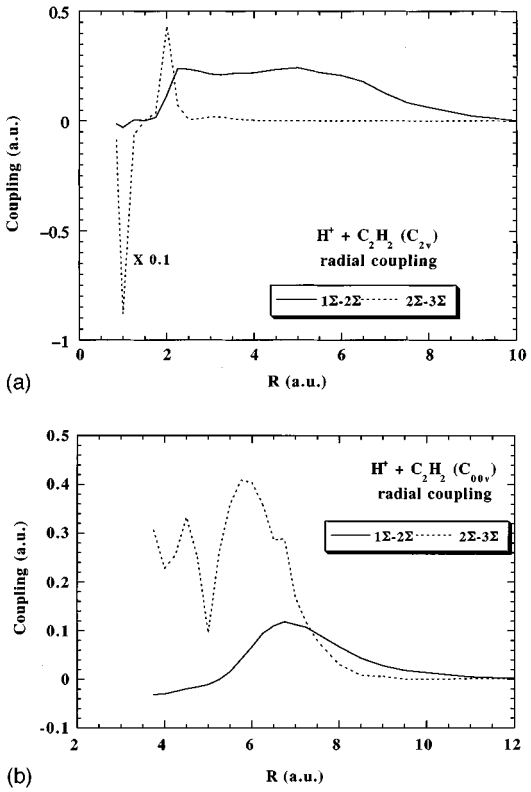

FIG. 2. (a) Representative radial couplings between the initial and electron-capture states for C_{2v} symmetry. (b) Representative radial couplings between the initial and electron-capture states for C_{00v} symmetry.

pattern of avoided crossings and hence, sharp coupling peaks. This qualitative difference in the couplings that occur for different molecular configurations is significant and should have an important influence on the collision dynamics exhibited by the H^+-C_2H_2 system.

B. Differential cross sections

1. General features

The differential cross sections obtained are shown in Figs. 3(a) and 3(b) and Figs. 4(a) and 4(b) both for C_{2v} and C_{00v} symmetries, for scattering angles $0°-180°$ at 1.5 and 0.5 keV, respectively. Both electron capture and direct elastic scattering are included. Several important features are summarized here and are discussed separately for small and large scattering angle regions for both energies: (i) $0\leqslant\theta<10°$ and (ii) $\theta\geqslant 10°$.

First for $0\leqslant\theta<10°$, the magnitude of the differential cross sections for electron capture in C_{2v} symmetry is slightly larger than that for C_{00v} symmetry in this scattering angle domain. Events resulting in scattering angles of 10° or smaller correspond roughly to those of impact parameters larger than $2.0a_0$. For such large impact parameters, the projectile does not interact strongly with any of the constituent atoms in C_{00v} symmetry, because the incoming H^+ ion just passes over the C_2H_2 molecule without strong interaction. By contrast, the projectile may feel a somewhat stronger effect from the C and H atoms for C_{2v} symmetry. Interestingly, as we shall see later, the total electron-capture cross

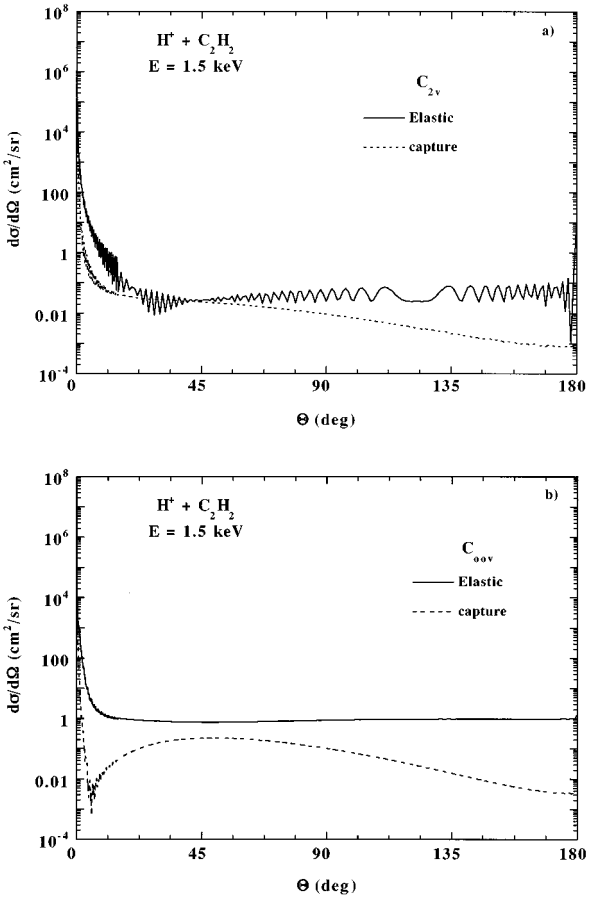

FIG. 3. (a) Differential cross section for C_{2v} at 1.5 keV. Solid line, elastic scattering; dashed line, electron capture. (b) Differential cross section for C_{00v} at 1.5 keV. Solid line, elastic scattering; dashed line, electron capture.

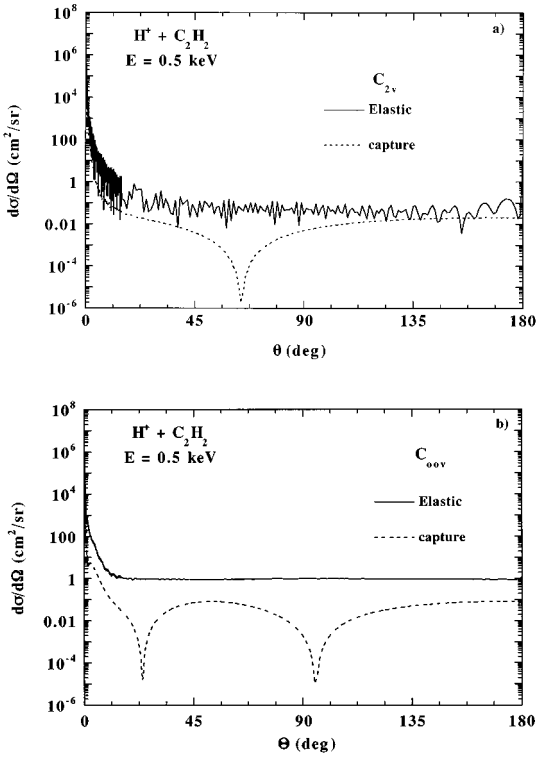

FIG. 4. (a) Differential cross section for C_{2v} at 0.5 keV. Solid line, elastic scattering; dashed line, electron capture. (b) Differential cross section for C_{00v} at 0.5 keV. Solid line, elastic scattering; dashed line, electron capture.

sections above 100 eV are larger by about a factor of 3–4 for C_{2v} symmetry than those for the linear approach. This is because near zero-angle scattering is responsible for most of the total cross section. In addition, the small, high-frequency oscillations apparent for C_{2v} symmetry in the elastic differential cross section may be attributable to quantum interferences. For C_{00v} symmetry, oscillatory structures are present, but they are much weaker. For electron-capture differential cross sections for both C_{2v} and C_{00v} symmetries, weak and irregular oscillatory structures are seen at small scattering angle below 10°.

Second, for $\theta \geqslant 10°$, the elastic differential cross section is smooth and flat, with a near-constant value of 1 cm^2/sr for a wide range of scattering angle (i.e., isotropic scattering) for C_{00v} symmetry, while that for C_{2v} symmetry has numerous irregular oscillations, but the mean value is nearly constant, with a small value of 0.1 cm^2/sr. These oscillations in C_{2v} symmetry are due to quantum interferences arising from strong two-state coupling. For C_{00v} symmetry, the isotropy is due to near head-on collisions between the projectile and an H atom in C_2H_2. For C_{00v} symmetry, one remarkable feature, i.e., a sharp dip in electron capture at 6° for 1.5 keV, which increases to two dips at 20° and 95° as the energy decreases to 0.5 keV, is due to rainbow scattering. For $\theta \geqslant 20°$, elastic scattering is always larger by at least an order of magnitude for C_{00v} symmetry, while for C_{2v} symmetry, elastic scattering is generally larger than electron capture for all scattering angles except in the 25°–45° region. These features are slightly changed as the energy decreases to 0.5 keV. The dip seen in electron capture for C_{00v} symmetry is not present in elastic scattering.

Third, at scattering angles near 180°, elastic-scattering differential cross sections rise rather sharply for C_{2v} symmetry, suggesting the occurrence of close collisions of the incoming H^+ ion with two carbon atoms at the center of the molecule [see Fig. 1(c)]. At much weaker degree, a similar trend of the rise in elastic-scattering differential cross section for C_{00v} symmetry can be seen, due to close collisions with a hydrogen atom in the end of the molecular chain. Regular continuous oscillatory patterns in the elastic cross section for C_{2v} symmetry are particularly interesting while a completely flat and nearly constant elastic cross section can be observed for C_{00v} symmetry. Except for the rise in the cross section near 180°, there is not much similarity between the two elastic cross sections.

2. Comparison with the $H^+ + H$ system

For C_{00v} symmetry in which the H^+ projectile directly approaches the H atom, it may be interesting to relate the present results with those for $H^+ + H$ collisions. In comparison with differential cross sections obtained below 1 keV for $H^+ + H$ collisions at scattering angle less than 6° [21] (although the present results for C_{00v} symmetry at the same energies and angles show qualitatively similar oscillatory patterns below 2° for both elastic and electron-capture processes), details are markedly different in several respects.

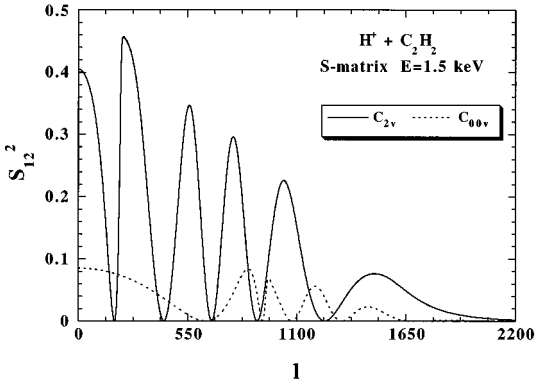

FIG. 5. Scattering S-matrix elements for C_{2v} and C_{00v} symmetries at 1.5 keV. Solid line, C_{2v}; dashed line, C_{00v}.

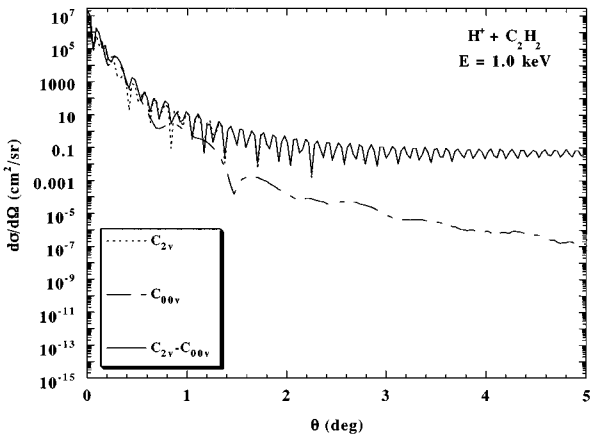

FIG. 6. Differential cross sections for electron capture for C_{2v}, C_{00v}, and C_{2v}-C_{00v} (interference) symmetries.

First, the $H^+ + C_2H_2$ differential cross sections are rather smoothly decreasing as a function of angle. But small oscillations occur more frequently than in $H^+ + H$; for example, there are roughly three main oscillations in $H^+ + C_2H_2$ collisions at $0.5° < \theta < 2°$ and 500 eV but only one oscillation in $H^+ + H$ collisions in the same angle region. Second, the differential cross section for electron capture in $H^+ + C_2H_2$ collisions is far smaller (by nearly 2 orders of magnitude) than that for elastic scattering, while these two processes are comparable in magnitude for $H^+ + H$. Third, at $\theta > 2°$, the present results for $H^+ + C_2H_2$ are nearly flat with numerous small oscillations, while oscillations for $H^+ + H$ appear to be damped within the model used. The origins of the oscillatory structures seen in $H^+ + H$ collisions have been thoroughly studied and are known to be due to combinations of interferences arising from (i) gerade-ungerade (g-u) electronic symmetry, (ii) minimum (or maximum) in the difference between the two adiabatic potential curves concerned, and (iii) the multichannel effect. For the present $H^+ + C_2H_2$ collisions, an electron on a H atom, combined with a $2p$ electron on the C atom, forms a covalent bond, changing the character of the isolated H atom significantly and hence destroying completely the g-u symmetry. This phenomenon may cause dissimilarity in differential cross sections, even though the molecular configuration of the collision appears to be similar in both cases. Since the C_2H_2 molecule is a linear molecule, unlike the previous CH_4 molecule, and the present molecular configurations considered do not explicitly include those causing multiple scatterings due to multiple centers of the molecule, the multiple-scattering effect, nevertheless, results in additional deviations from simpler $H^+ + H$ collisions.

It should be very interesting and educational to compare the present results with those of *positron* impact, i.e., $e^+ + C_2H_2$ collisions, since both projectiles share the same positive charge. However, to the best of our knowledge, there is no experimental measurement on differential cross sections for the C_2H_2 target based on positron impact, and this is quite unfortunate.

Figure 5 displays scattering S-matrix elements for the two symmetries at the collision energy of 1.5 keV. The close examination of the S-matrix elements may provide further information of the collision dynamics and here, several points observed are noteworthy: (i) the S-matrix element for C_{2v} symmetry has regularly oscillatory structures with three peaks between $l = 0$ and 550, while that for C_{00v} symmetry has no oscillatory structures for l smaller than 550 followed by small four oscillations before it completely becomes zero beyond $l = 2000$; (ii) the height of each peak gradually decreases for C_{2v} symmetry as l increases and, hence, on overall profile of the S matrix for this configuration shows a bell-shape as a function of l, while that does not decrease for C_{00v} symmetry as l increases until it reaches the last peak. The difference of the molecular configurations is responsible for these features, in which for C_{00v} symmetry the close collision is more probable and, hence, the contribution from wider l values is equally significant. No oscillation in the S matrix at smaller l values for C_{00v} symmetry is, again, the manifestation of the close collision. For C_{2v} symmetry, as l increases, which corresponds to larger impact parameters from the midpoint of the C-C bond in the target where the most charge distribution concentrates, the charge distribution decreases gradually reflecting the smooth decrease of the magnitude of the S-matrix element. As the energy decreases, these aspects of the S-matrix elements are more enhanced.

C. Interferences between different molecular orientations

As Figs. 3 and 4 show, the differential cross sections for C_{2v} and C_{00v} symmetries have conspicuous differences in shape and magnitude as discussed in detail above. However, in a usual experimental setup, the measurement is conducted under the condition where molecular geometries are not fixed with a specific configuration, and hence, measured cross section is obtained as an averaged cross section over contributions from all molecular configurations. Therefore, for a proper comparison of the present result with experimental measurement, it is necessary to take some sort of an averaging procedure. By employing a coherent sum of two scattering amplitudes, we can obtain differential cross section that may be compatible with the one experimentally measurable. From a theoretical point of view, by taking this approach, we can examine the interference between different molecular configurations in the collision dynamics. Care should be taken, however, that the present calculated result is not a quantitative prediction of an actual experiment because in a real measurement, all molecular configurations are included for averaging, not just two molecular configurations

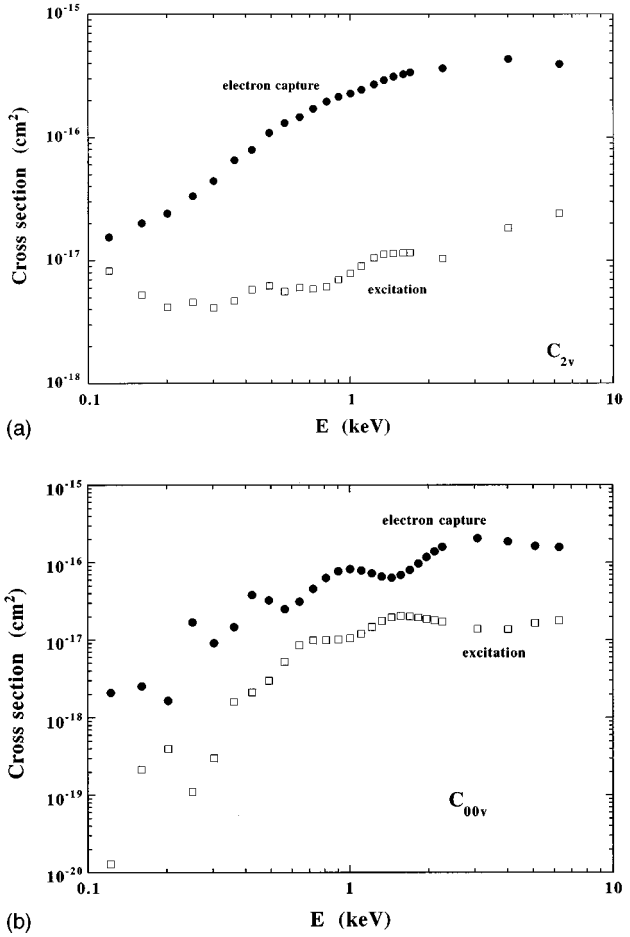

FIG. 7. Total electron capture cross sections for (a) C_{2v} and (b) C_{00v} symmetries.

as considered here. The results based on this approach are shown in Fig. 6 for C_{2v}, C_{00v}, and C_{2v}-C_{00v} configurations for scattering angles from 0° to 5° at 1 keV. As pointed out earlier, since differential cross sections in both configurations are found to be similar in magnitude at small angle regions only, two cross sections there are expected to strongly interfere with each other and distinct interference patterns become evident. At angles below 1°, the strongest interference can be seen in the figure and as the angle increases from 1°, the differential cross section in C_{2v} symmetry is dominant and correspondingly, that for C_{2v}-C_{00v} symmetry becomes identical to that for C_{2v} symmetry. Because of the interference, one can observe that some oscillatory structures seen are now out of phase between those of C_{2v} and C_{2v}-C_{00v} symmetries. Since the depth of oscillations is rather large, experimentally, this could be observable if properly conducted. Again, an experimental result for this system is urgently required for rigorous comparison.

D. Total cross sections

Total cross sections obtained by using the semiclassical calculation are illustrated separately for C_{2v} and C_{00v} symmetries in Figs. 7(a) and 7(b). As stated, contributions from all channels, which are electron-capture (EC), electron-capture with simultaneous target excitation (ECTE), and target excitation (TE), are included separately along with the summed total cross section in both symmetries. Total electron capture for the C_{2v} approach appears to possess the minimum at the lowest energy studied near the 30–40-eV region, and gradually increases as the energy increases, reaching a maximum value of 4.5×10^{-16} cm^2 around 4 keV, while that for C_{00v} also increases just above the threshold and reaches a maximum, with a value of 2×10^{-16} cm^2 around 3 keV. The contribution from 1Σ (EC) drops as the energy decreases, while that from 3Σ (ECTE) gradually increases, hence resulting in the minimum in the total cross section for C_{2v}, symmetry as seen. The total cross section for C_{2v} symmetry is rather smooth as a function of energies while that for C_{00v} symmetry has strong oscillatory structures in the entire energy region. These features are the manifestation of the coupling matrix elements and coupling schemes (Landau-Zener versus Demkov) discussed earlier (see also Fig. 2 for the coupling matrix elements). Cross sections for EC and ECTE are found to have out-of-phase oscillatory structures for C_{00v} symmetry, while that for EC is solely dominant above 0.2 keV and ECTE takes over below this energy in C_{2v} symmetry. There is no experimental measurement on total cross section of this system, to the best of our knowledge. However, Tawara [22] measured electron capture cross sections from C_2H_2 by C^+ impact above 0.2 keV. Their measurements seem to be larger by a factor of 2 than the present result in magnitude above 1 keV, but their energy dependence of the cross section appears to be in good harmony. Below 1 keV, their results begin to increase after the minimum, while the present result starts to show an increase at much lower energies below 0.2 keV as seen in Fig. 7. For the C^+ projectile, more capture channels are available within narrow energy separations, compared to the H^+ projectile, and hence, this trend of a rise in the cross section at relatively higher energy may be understandable.

E. Contributions of TE and higher excited levels

The effect of higher-lying excited levels was also examined for the linear and perpendicular H^+ approaches. As shown in Fig. 7, these results help one to understand dynamics well and to establish the level of convergence in our calculations. As discussed, EC to the ground $[H+C_2H_2{}^+]$ state is dominant in both symmetries below a few keV, and remains so until the collision energy gets down to approximately 0.25 keV for C_{2v} symmetry, and for any low energy in C_{00v} symmetry. Contributions from ECTE are somewhat small and have been discussed in detail above. Hence, a two- or three-channel approximation would be appropriate for obtaining reasonably converged results for the present energy region of interest. TE for C_{2v} symmetry becomes dominant below 0.14 keV, while it is still secondary for C_{00v} symmetry. Furthermore, TE and EC and ECTE in C_{00v} symmetry show much stronger out-of-phase oscillations than those in C_{2v} symmetry within certain limited energy regions. These different features of TE are a reflection of the difference of adiabatic potentials in each symmetry, namely, for C_{2v} symmetry, the TE channel lies two levels above the initial channel, while that for C_{00v} symmetry is separated by three channels from the initial one. Also, the initial channel for C_{2v} symmetry possesses a strong mixing of states below $R<2.8$ a.u., resulting in stronger coupling matrix elements

and hence, flux transfer. This difference in the TE process between the two symmetries is noteworthy.

F. Dissociation fragmentations

Since the first ionization potential of the acetylene molecule is 11.41 eV [18], the lowest dissociation limit for the protonated system is $[C_2H_2{}^+(^2\Pi)+H(^2S)]$. The next most stable products are $[C_2H_2(^1\Sigma_g)+H^+]$, lying 2.19 eV higher in energy. The present calculations overestimate this energy difference by 0.20 eV. The third most stable set of dissociation products again involves $C_2H_2{}^+$, in this case in its $^2\Sigma$ excited state. The $^2\Sigma$-$^2\Pi$ transition energy is computed to be 5.95 eV. The next lowest asymptotes of protonated C_2H_2 correspond to excited states of the neutral molecule. Experimentally the first such state is found to have a *trans* nuclear conformation with a relatively small equilibrium angle of 120° [18], but it does not play a key role in the scattering processes in which there is little time for the acetylene molecule to relax. For the present purposes, the next lowest-energy states of interest are the $\pi\rightarrow 3s\,^{3,1}\Pi_u$, both of which are linear, with only a slightly larger C—C bond length than in the C_2H_2 ground state. The T_0 value of the singlet is 8.16 eV [23]. The present CI calculations for the isolated C_2H_2 molecule are in good agreement with this result, but it is found that the effect of the colliding proton is quite significant, even at relatively large internuclear separations. The stabilization energy is 0.73 eV, for example, when the proton is located $10.0a_0$ from the midpoint of the C_2H_2 molecule in its experimental equilibrium geometry (C_{2v} approach). The corresponding wave function is strongly perturbed at this distance as well. It is quite easy to distinguish the valence and Rydberg states of neutral C_2H_2 of this basis.

IV. SUMMARY

Theoretical study of elastic and electron-capture processes in collisions of H^+ ions with C_2H_2 molecules in the energy range from 30 eV to 1.5 keV was carried out for two distinct molecular orientations, the C_{2v} and C_{00v} symmetries, by using a molecular-orbital expansion method with six- and three-channel molecular states within semiclassical and quantum-mechanical formalisms, respectively. Collision dynamics for C_{2v} and C_{00v} symmetries were found to be effective in nearly the same small scattering-angle regions. Hence, the interference arising from these two molecular configurations occurs rather strongly at small regions of scattering angle, and unambiguous structures in differential cross sections arising from the interference are observed. The integrated cross section for electron capture in C_{2v} symmetry is found to have the value of 4.5×10^{-16} cm^2 at 4 keV. The general qualitative tendency of the cross section is in reasonable accord with the similar measurement using C^+ ion impact for the present target in the energy region they overlap although the magnitude of the cross section is markedly different. We extend the present study to examine the fragmentation products and also to study dynamics for other molecular targets such as C_2H_4 and C_2H_6.

ACKNOWLEDGMENTS

The work was supported in part by the U.S. Department of Energy, Office of Basic Energy Sciences through Rice University, and by the Deutsche Forschungsgemeinschaft (Grant Be:450/7). The financial support of the Fonds der Chemischen Industie is also hereby gratefully acknowledged (Y.L., G.H., and R.J.B.). The authors acknowledge Dr. Tawara for useful discussions.

[1] M. Kimura and N. F. Lane, in *Advances in Atomic and Molecular Physics*, edited by D. R. Bates and B. Bederson (Academic, New York, 1989), Vol. 26, p. 79.
[2] W. Fritsch and C. D. Lin, Phys. Rep. **202**, 1 (1991).
[3] M. Kimura, Phys. Rev. A **32**, 802 (1985).
[4] R. Shingal and C. D. Lin, Phys. Rev. A **40**, 1302 (1989).
[5] W. Fritsch, Phys. Rev. A **46**, 3910 (1992).
[6] M. B. Shah and H. B. Gilbody, J. Phys. B **11**, 121 (1978).
[7] D. Čičiň, D. Dijkkamp, E. Vliegad, and F. J. de Heer, J. Phys. B **18**, 4745 (1985).
[8] R. Hoekstra, Ph.D. thesis, University of Groningen, 1990 (unpublished).
[9] M. Kimura, Y. Li, G. Hirsch, and R. J. Buenker, Phys. Rev. A **52**, 1196 (1995).
[10] F. Schneider, A. Palma, E. Semprini, and F. A. Gianturco, J. Chem. Phys. **99**, 1985 (1993).
[11] R. J. Buenker and S. D. Peyerimhoff, Theor. Chim. Acta **35**, 33 (1974); **39**, 217 (1975); R. J. Buenker, Int. J. Quantum Chem. **29**, 435 (1986).
[12] R. J. Buenker, in *Proceedings of the Workshop on Quantum Chemistry and Molecular Physics, Wollongong, Australia*, edited by P. Burton (University Press, Wollongong, 1980).
[13] S. Huzinaga, J. Chem. Phys. **42**, 1293 (1965).
[14] T. H. Dunning, Jr., J. Chem. Phys. **53**, 2823 (1970).
[15] E. R. Davidson, in *The World of Quantum Chemistry*, edited by R. Daudel and B. Pullman (Reidel, Dordrecht, 1974), p. 17.
[16] R. J. Buenker, D. B. Knowles, S. N. Rai, G. Hirsch, K. Bhanuprakash, and J. R. Alvarez-Collado, in *Studies in Physical and Theoretical Chemistry*, edited by R. Carbo (Elsevier, Amsterdam, 1989), Vol. 62, p. 181.
[17] D. B. Knowles, J. R. Alvarez-Collado, G. Hirsch, and R. J. Buenker, J. Chem. Phys. **92**, 585 (1990).
[18] G. Herzberg, *Molecular Spectra and Molecular Structure* (Van Nostrand Reinhold, New York, 1966), Vol. III.
[19] See details of collision theory, for example, B. H. Bransden, *Atomic Collision Theory* (Benjamin, New York, 1983).
[20] R. E. Olson and F. T. Smith, Phys. Rev. A **3**, 1607 (1971).
[21] M. Kimura, Ph.D. thesis, University of Alberta, 1981 (unpublished). Also see R. Schinke and H. Kruger, J. Phys. B **9**, 2469 (1976).
[22] H. Tawara (unpublished).
[23] P. G. Wilkinson, J. Mol. Spectrosc. **2**, 387 (1958).